Published in final edited form as:
Cell Rep. 2012 December 27; 2(6): 1684–1696. doi:10.1016/j.celrep.2012.10.021.

FGF regulates TGFβ signaling and endothelial-to-mesenchymal transition via control of *let-7* miRNA expression

Pei-Yu Chen[1,*], **Lingfeng Qin**[2,*], **Carmen Barnes**[3,#], **Klaus Charisse**[3], **Tai Yi**[2], **Xinbo Zhang**[1], **Rahmat Ali**[2], **Pedro P. Medina**[4], **Jun Yu**[1], **Frank J. Slack**[4], **Daniel G. Anderson**[5,6,7], **Victor Kotelianski**[5], **Fen Wang**[8], **George Tellides**[2], and **Michael Simons**[1,9]

[1]Yale Cardiovascular Research Center, Section of Cardiovascular Medicine, Department of Internal Medicine, Yale University School of Medicine, New Haven, CT 06520, USA

[2]Department of Surgery, Yale University School of Medicine, New Haven, CT 06520, USA

[3]Alnylam Pharmaceuticals Inc., 300 3rd street, Cambridge, Massachusetts 02142, USA

[4]Department of Molecular, Cellular and Developmental Biology, Yale University, New Haven, CT 06520, USA

[5]Department of Chemical Engineering, Massachusetts Institute of Technology, Cambridge, MA 02139

[6]David H. Koch Institute for Integrative Cancer Research, Massachusetts Institute of Technology, Cambridge, MA 02139

[7]Harvard-MIT Division of Health Science and Technology, Massachusetts Institute of Technology, Cambridge, MA 02139

[8]Texas A&M Health Science Center, Houston, TX 77030, USA

[9]Department of Cell Biology, Yale University School of Medicine, New Haven, CT 06520, USA

Summary

Maintenance of normal endothelial function is critical to various aspects of blood vessel function but its regulation is poorly understood. In this study we show that disruption of baseline FGF signaling to the endothelium leads to a dramatic reduction in *let-7* miRNA levels that in turns increases expression of TGFβ ligands and receptors and activation of TGFβ signaling leading to endothelial-to-mesenchymal transition (Endo-MT). We further find that Endo-MT is an important driver of neointima formation in a murine transplant arteriopathy model and in rejecting human transplants lesions. The decline in endothelial FGF signaling input is due to the appearance of an FGF resistance state that is characterized by inflammation-dependent reduction in expression and

Address correspondence to: Michael Simons, MD, Section of Cardiovascular Medicine, P.O. Box 208017, 333 Cedar Street, New Haven, CT 06520-8017, Phone: 203-785-7000, michael.simons@yale.edu.
*Equal contribution
#Current address: Celgene Avilomics Research, Bedford, MA.

Author contributions

P-Y.C, L.Q, G.T, and M.S. conceived and designed the experiments and discussed the results. P-Y.C, L.Q., T.Y., X.Z., R.A., and J.Y. performed experiments. P.P.M. and F.J.S. generated and provided *let-7* sponge construct, F.W. generated FRS2 knock-in mouse, and C.B, K.C., D.G.A., and V.K. developed in vivo delivery system and generated and provided *let-7* anti-miRs for in vivo studies. P-Y.C., G.T. and M.S. wrote the manuscript.

activation of key components of the FGF signaling cascade. These results establish FGF signaling as a critical factor in maintenance of endothelial homeostasis and point to an unexpected role of Endo-MT in vascular pathology.

Introduction

Maintenance of the normal vasculature is an active process. Fibroblast growth factors (FGF) have recently emerged as key regulators of the normal vascular state (Hatanaka et al., 2010; Murakami et al., 2008). Circulating and tissue-resident FGF signal via cognate tyrosine kinase receptors that require the intracellular adaptor FRS2 for the initiation of MAPK signaling (Eswarakumar et al., 2005). Experimental evidence using various in vitro models points to FGF's role in inhibition of TGFβ signaling. Thus, FGF2 downregulates TGFβR1 expression, attenuates endothelial cell (EC) responses to TGFβ (Fafeur et al., 1990) and antagonizes TGFβ1-mediated smooth muscle α-actin (αSMA) expression (Papetti et al., 2003). In addition, FGF can revert TGFβ1-induced epithelial-to-mesenchymal transition (EMT) in epithelial cells via the MAPK pathway (Ramos et al., 2010). These observations suggest that loss of endothelial FGF signaling may lead to upregulation of the TGFβ pathway and promotion of adverse changes in the vasculature. However, the molecular mechanisms linking FGF and TGFβ signaling cascades and the biological role of FGF-dependent regulation of TGFβ signaling have not been identified.

One likely consequence of dysregulated TGFβ signaling in the vasculature is the development of neointima. Neointima formation underlies a number of common diseases including transplant vasculopathy, post-angioplasty and vascular graft restenosis, hypertension, and atherosclerosis among others. Despite decades of investigations, the origins of neointimal cells still remains controversial with studies variously pointing to the role of medial smooth muscle cell (SMC) proliferation (Costa and Simon, 2005), vessel wall inflammation (Ohtani et al., 2004) and adventitial angiogenesis (Khurana et al., 2004).

One potential contributor to neointima formation is the process of endothelial-to-mesenchymal transition (Endo-MT). Somewhat similar to EMT, Endo-MT is thought to result in endothelial cells trans-differentiating into mesenchymal cell types, including SMC-like and fibroblast-like cells. While Endo-MT has been implicated in several pathological processes including cardiac fibrosis (Zeisberg et al., 2007b) and pulmonary hypertension (Kitao et al., 2009), its very existence is still controversial. Similarly to EMT, Endo-MT is thought to be driven by TGFβ in a Smad-dependent and independent manner (Kitao et al., 2009; Medici et al., 2011). However, factors leading to Endo-MT under pathologic conditions or suppressing its occurrence in the normal vasculature have not been identified.

In this study we observed that a shutdown of endothelial FGF signaling in normal EC results in increased expression of TGFβ ligands and receptors and activation of TGFβ signaling. In vitro this resulted in a change in EC morphology and expression of SMC markers. In vivo, using fate-mapped mice, we observed neointima formation and extensive perivascular fibrosis. The process was driven by a decline in endothelial expression of *let-7* miRNAs that normally maintain low levels of TGFβR1 expression. The effects of FGF signaling shutdown on Endo-MT induction could be mimicked by inhibition of *let-7b* or *let-7c* expression in vitro and in vivo. Endo-MT was a critical driver of neointima formation in a transplant arteriopathy model in mice, was present in rejecting human transplants and could be reversed by treatment with *let-7*b mimics. These results demonstrate that basal FGF signaling is required to maintain high *let-7* expression in the endothelium that in turn prevents activation of TGFβ signaling and suppresses Endo-MT.

Results

1. Basal FGF signaling suppresses TGFβ-mediated Endo-MT

To test the role of FGF signaling in EC, we used RNA interference in human umbilical artery endothelial cells (HUAEC) to inhibit expression of FRS2, the key adaptor molecule involved in FGF receptors signaling. Immunofluorescence staining showed that while control HUAEC display a typical rounded/cobblestone morphology, FRS2 knockdown resulted in a distinct change in cell shape accompanied by expression of smooth muscle calponin (SM-calponin), a protein not normally expressed in the endothelium (Fig. 1A). Western blotting confirmed the appearance of this and other SMC markers in FRS2 knockdown cells (Fig. 1B). FACS analysis showed that both control and FRS2 knockdown EC expressed CD31 and were able to take up Di-acLDL, ruling out SMC contamination (Fig. 1C).

These findings suggest that following FRS2 knockdown EC are undergoing Endo-MT as defined by an acquisition of mesenchymal markers. Since TGFβ signaling has been implicated in this process, we next examined TGFβ-related gene expression. qPCR analysis demonstrated a marked increase in TGFβ1 and TGFβ2, all three TGFβ receptors, as well as several collagen isoforms and other matrix proteins that are stimulated by TGFβ signaling (Fig. 1D, E). Western blotting confirmed increased TGFβR1 expression and activation of TGFβ signaling (Fig. 1F). To verify that disruption of FGF signaling induces TGFβ signaling and Endo-MT, HUAEC were transduced with mutant forms of FRS2 that inhibit FGF signaling or with a dominant negative FGFR1 (FGFR1-DN, Fig S1A). A complete suppression of FGF signaling achieved with expression of FGFR1-DN or FRS2α-6F constructs resulted in increased TGFβ signaling (Fig S1B) and an increase in smooth muscle and other mesenchymal marker expression (Fig. S1C).

To demonstrate that activation of TGFβ signaling following FRS2 knockdown is indeed necessary and sufficient for Endo-MT, several different experimental approaches were used. Treatment of FRS2 knockdown EC with the TGFβR1 inhibitor SB431542 significantly decreased SM-calponin, fibronectin and vimentin expression (Fig. 1G). Similar results were seen after transduction of a dominant negative TGFβR1 construct (TGFβR1 K230R) (Fig 1H) while silencing Smad2 expression with a specific shRNA resulted in a significant decrease in SM-calponin, but not in fibronectin and vimentin expression (Fig 1I). Finally, activation of TGFβ signaling in the absence of FGF signaling suppression was achieved by introduction of the wildtype TGFβR1 together with TGFβ or by expression of a constitutively active TGFβR1 (TGFβR1-T202D) into HUAEC with a kinase dead mutant TGFβR1-K230R used as a control (Fig S2A,B). Thus achieved, activation of TGFβ signaling resulted in increased expression of smooth muscle (Fig S2C) and other mesenchymal markers (Fig S2D).

2. FGF controls TGFβR1 signaling via regulation of *let-7* miRNA expression

We next examined the mechanism responsible for increased expression of TGFβR1 following FGF signaling shutdown. Analyses of mRNA half-life showed a marked increase following a knockdown of FRS2 expression (Fig. 2A). This suggests the presence of miRNA regulating TGFβR1 message stability. In silico analysis identified binding sites for the *let-7* family of miRNAs with an exact match to the seed sequence of *let-7* in TGFβR1 3'-UTR 75–82 and 3889–3895 (Fig. 2B). At the same time, miRNA array analysis demonstrated a >20 fold reduction in expression of all *let-7* family members (with *let-7b* and *7c* reduced 108 and 120 fold, respectively) following FRS2 knockdown in EC (Fig. 2C).

To demonstrate that increased TGFβ signaling following FGF suppression is directly due to changes in *let-7* levels, we inhibited *let-7* expression using two alternative approaches.

Transduction of human umbilical vein endothelial cells (HUVEC) with Lin28, a known regulator of *let-7* biogenesis during embryonic development (Viswanathan and Daley, 2010), resulted in increased expression of genes in the TGFβ pathway and smooth muscle and mesenchymal markers (Fig 2D, left panel and Fig S3). Similarly, HUVEC transduction with a *let-7* "microsponge" construct that effectively suppresses expression of all *let-7* miRNAs also led to a marked increase in TGFβR1, SM-calponin and HMGA2 (a known *let-7* target) expression (Fig. 2D, right panel).

We then examined if restoration of *let-7* expression in EC with suppressed FGF signaling would in turn inhibit activation of TGFβ signaling and Endo-MT induction. To this end, HUAEC were transduced with *let-7*b or *let-7*c pre-miRs. Increased TGFβR1 expression and Smad2 phosphorylation induced by FRS2 knockdown were completely reversed by transduction with either *let-7*b or *let-7*c as was the expression of all Endo-MT markers (Fig. 2E,F).

The link between FGF signaling and *let-7* expression was then studied in vivo. Replacement of specific tyrosines in FRS2 (FRS2α-2F, Fig S1A) that are phosphorylated by FGF biding to FGFR1 and activate ERK signaling results in a marked reduction in FGF signaling and embryonic lethality (Gotoh et al., 2004). Examination of FRS2α-2F embryos at E10.5 demonstrated a gene dose-dependent reduction in *let-7* levels (Fig S4A).

FGF signaling in adult mice can be inhibited by administration of an FGF trap construct (sFGFR1-IIIC) (Murakami et al., 2008). To demonstrate construct effectiveness, exposure of cultured HUVEC to Ad-sFGFR1-IIIc resulted in a distinct morphological change (Fig S4B), suppression of *let-7* expression (Fig S4C), and induction of Endo-MT markers including SM22α, SM-calponin and fibronectin (Fig S4D,E). In agreement with these in vitro data, Ad-sFGFR1-IIIc injection into mice led to their detection in the host circulation and a significant reduction in *let-7* miRs expression in primary EC isolated from hearts and livers of these animals (Fig S4F,G).

To determine if reduction in *let-7* expression would have the same effects in vivo as suppression of FGF signaling, we directly targeted *let-7*b and *let-7*c miRNAs in mice using cholesterol formulated antagomirs for improved stability and delivery efficiency (Love et al., 2010). Analysis of *let-7* miRNAs expression six days after a single tail vein injection of 2 mg/kg of *let-7*b/c antagomirs in primary liver EC demonstrated a significant reduction in expression of *let-7*b and *let-7*c miRNA in antagomir-treated compared to control mice while other family members were not affected (Fig. 2G). This reduction in *let-7*b/c levels was further confirmed by increased expression of several known *let-7* targets including K-ras, N-ras, HMGA2, CDK6 and CDK25A (Fig 2H). In agreement with the in vitro data, reduction in *let-7*b/c expression led to an increase in TGFβR1 and vimentin expression (Fig 2H). Finally, immunocytochemical examination of blood vessels in the liver of *let-7* antagomir-treated mice demonstrated increased expression of vimentin in luminal EC, consistent with Endo-MT (Fig 2I,J).

3. Inflammation-dependent suppression of FGF signaling

The results of the in vitro and in vivo studies presented above demonstrate that decreased FGF signaling leads to reduction in *let-7* expression and initiation of TGFβ-dependent Endo-MT. To demonstrate the relevance of this biology to disease settings, we next examined if Endo-MT occurs in transplant rejection, a process associated with high local interferon-γ (IFN-γ) production that has been reported to suppress FGF signaling (Friesel et al., 1987).

Treatment of HUVEC in culture with IFN-γ led to increased expression of a *let-7* dependent gene HMGA2, an increase in TGFβR1 and Smad2 levels and a large increase in the expression of SMC and other mesenchymal marker expression, including Notch3, SM22α, fibronectin and vimentin (Fig. 3A,B). Of note there was a profound reduction in FGFR1 expression and almost full suppression of FGF signaling (Fig 3C). Treatment of EC with TNF-α and IL-1β led to a similar reduction in FGF signaling (Fig 3C) while other inflammatory cytokines such as IL-6, MCP-1 and VEGF had no such effect (Fig. S5A–C). In agreement with the observed reduction of FGF signaling, exposure of HUVEC to IFN-γ led to a profound decrease in *let-7* miRs expression (Fig. 3D).

We next employed a mouse transplant rejection model characterized by intense local inflammatory responses around the rejecting graft and endothelial fate mapped mice that were generated by crossing Cdh5-CreER2 and mT/mG ("tomato") mouse lines (both on a C57BL/6 background) followed by activation of the Cre gene by tamoxifen administration from P2 to P20 (Fig S6A). This results in permanent marking of all EC and EC-derived cells with GFP. Analysis of arteries from these mice demonstrated uniform GFP expression in the luminal EC with a total absence of all SMC (Notch3, αSMA, SM22α) or mesenchymal (vimentin, collagen) markers (Fig S6B).

Engraftment of an aortic segment from BALB/c mice into Cdh5-CreERT2-mT/mG (C57BL/6 background) mouse aorta leads to intense graft inflammation and rejection over the next 2–3 weeks. To test the effect of this inflammatory response on endothelial FGF signaling, the mouse hosts of allogeneic artery grafts were intravenously injected with FGF2 at 2 weeks postoperatively and sacrificed 15 min later. Immunocytochemical analysis for FGF signaling demonstrated virtually no p-ERK signal in graft luminal EC while luminal EC from the adjacent normal arterial segment revealed intense p-ERK signal (Fig 3E).

Examination of the graft 2 weeks after transplantation showed that 10.1% of neointimal SMC (defined by expression of either Notch3 or αSMA) expressed GFP which indicated an endothelial origin (Fig 4A,B). Furthermore, a very high proportion of EC in the neointima (79%) expressed Notch3 and αSMA (Fig 4A,C), demonstrating very extensive Endo-MT. To examine the effect of FRS2α expression disruption on this process, we crossed FRS2α$^{fl/fl}$ mice onto mT/mG background. FRS2α expression was then inactivated by crossing these mice with Cdh5-CreERT2 driver line (iEC-FRS2α$^{-/-}$) and then activating Cre expression on post-natal day 5 (P5).

Inhibition of FGF signaling by endothelial-specific FRS2α deletion or suppression of *let-7* expression with antagomirs resulted in a further statistically significant ($p<0.05$) increase in the number of GFP^{+} SMC (Fig 4A,B) while the proportion of neointimal EC with SMC markers increased to nearly 100% (Fig 4C).

Luminal EC revealed even more extensive changes: 61% of graft lumen EC expressed Notch3 and αSMA with the extent of Endo-MT increasing to 80–90% in iEC-FRS2α$^{-/-}$ mice or following *let-7* anti-miR administration (Fig 4D). Collagen deposition, another feature of Endo-MT, and neointima thickness of transplanted arteries were significantly increased by both endothelial cell FRS2α deletion and *let-7* antagomir treatment (Fig 4E,F).

To test the ability of *let-7* miR to rescue this phenotype we used chemically synthesized double stranded *let-7*b miR mimics packaged in liposomal-formulated lipid nanoparticles (LNPs) (Love et al., 2010). The effectiveness of delivery against endothelial targets was assessed by first determining the dose response for inhibition of target gene expression. A single intravenous injection of LNPs carrying from 0.03 to 2.2 mg/kg of anti-Tie2 siRNA demonstrated 70% inhibition of *Tie2* expression in liver and heart EC after 72 hr (Fig S7A,B) persisting with ~30 day half-life in both organs (Fig S7C,D). Similar results were

seen with siRNA formulations targeting *Icam2* (Fig S7E,F), *Vegfr2* (Fig S7G,H) and Cdh5 (Fig S7I,J). In contrast, no detectable reduction of any tested gene was observed with a LNP-formulated luciferase siRNA (LUC) or saline (Fig S7A,B,E–J), indicating that silencing is specific to the siRNA and is not caused by the liposomal carrier. To demonstrate the physiological significance of this level of inhibition, we carried out an Evans blue assay in mice treated with 0.7 mg/kg of LNP Cdh5 siRNA. Following knockdown, there was a significant increase in EC permeability compared to control mice (Fig S7K).

Using the LNP preparation described above, *let-7* mimics (0.5 mg/kg) were injected every other day starting at postoperative day 7 (for a total of four injections) and the grafts were harvested on day 14. Administration of these mimics to grafted mice led to a significant reduction in the number of neointimal SMC of endothelial origin (GFP^+/$Notch3^+$ or αSMA^+ cells: from 10.1% in the absence of treatment to 3% in mimic-treated mice, $p<0.05$) (Fig 4A,B) as well as in the proportion of neointimal EC undergoing Endo-MT (from 79% to 20.3%, $p<0.01$; Fig 4A,C). Equally significantly, there was a dramatic decrease in the proportion of luminal EC undergoing Endo-MT (from 61% to 33.7%, $p<0.01$; Fig 4A,D) and a dramatic reduction in collagen deposition and neointima thickness (Fig 4A,E,F)

To determine if a similar phenomenon occurs in human disease, we examined coronary arteries (n=8) from explanted chronically rejecting hearts. Compared to normal human coronary arteries (Fig 5A), the majority (79.8%) of luminal EC in arteries procured from patients with chronic cardiac graft rejection expressed the SMC marker, Notch 3 (Fig 5B,C,E). Analysis of the neointima showed that similar to the mouse transplant model, Endo-MT was extensive with 76% of neointimal EC expressing Notch3 (Fig 5D,F) and accounted for a significant portion (9.6%) of neointimal SMC (Fig 5G).

Transplantation of a segment of human coronary artery into immunodeficient mouse aorta reconstituted with allogeneic human PBMC to induce graft rejection (Rao et al., 2008) was then used to verify the occurrence of Endo-MT in human endothelium. Three weeks following PBMC injection, rejecting human arteries demonstrated extensive neointima formation (compare Fig 5 H vs. I) and widespread expression of Notch3 in luminal and neointimal EC (Fig 5J,K). Quantitative analysis demonstrated that 84.7% of all luminal and 77% of neointimal EC expressed Notch3 (Fig 5L,M) while 10.4% of neointimal SMC expressed EC markers (Fig 5N).

Finally, to examine the frequency of this phenomenon in other settings, we evaluated two other in vivo models characterized by various extents of neointima formation and vascular inflammation- wire injury and vein-to-artery grafting. Wire injury to the common femoral artery in Cdh5-CreERT2;mT/mG mice resulted in neointima development with 5.2% of neointimal cells demonstrating GFP expression (Fig 6A). Grafting mouse vena cava into the aorta of syngeneic Cdh5-CreERT2;mT/mG mice was also associated with evidence of Endo-MT in the neointima 3% at 2 weeks and 6.7% at 4 weeks. Luminal EC of the vein graft also displayed extensive Endo-MT with 31% expressing mesenchymal markers 2 weeks after grafting and 45.6% after 4 weeks (Fig 6B).

Discussion

The data in the present study indicate that basal FGF signaling in EC is required to maintain *let-7* miRNA expression. High *let-7* levels, in turn, are required for suppression of TGFβ signaling and inhibition of Endo-MT. Finally, Endo-MT itself is an important contributor to the development of neointima in a number of disease states characterized by FGF signaling resistance. Thus, FGF control of *let-7* expression directly regulates TGFβ signaling, links

these two critical growth factor signaling pathways, and maintains the normal state of the vasculature (Fig 7).

FGFs exert a plethora of effects on a large number of cell types (Eswarakumar et al., 2005). In the vascular system FGF signaling plays a protective role with ongoing FGF stimulation required for the maintenance of vascular system integrity (Hatanaka et al., 2010; Murakami et al., 2008) and VEGFR2 expression (Murakami et al., 2011). The current study expands this novel FGF function by demonstrating the role of ongoing FGF signaling in prevention of Endo-MT and implicates *let-7* miRNA as the key player in this process.

let-7 miRNA family was originally identified in *C. elegans* as a regulator of developmental timing and cell proliferation (Reinhart et al., 2000). The family is highly conserved across the entire phylogenetic tree and in mice and humans it consists of 11 very closely related genes encoded on three different chromosomes (Roush and Slack, 2008). To date, *let-7* miRs have been implicated in the control of numerous events during embryogenesis including nervous system and liver development (Maller Schulman et al., 2008), tumor suppression (Zhang et al., 2007) and inhibition of cell proliferation (Johnson et al., 2007) while recent studies have indicated their involvement in EMT in tumors including a suggestion that an increase in *let-7*b levels reverses this process (Li et al., 2009). *let-7* miRNAs are also highly expressed in EC and are considered pro-angiogenic (Urbich et al., 2008).

Despite these important biological roles, little is known about the regulation of *let-7* biogenesis. During embryonic development RNA binding proteins Lin28a/b selectively block its maturation (Hagan et al., 2009; Lehrbach et al., 2009) while a heteronuclear ribonucleoprotein A1 (hnRNPA1) inhibits its processing by Drosha (Michlewski and Caceres, 2010). Lin28 is not expressed in the adult endothelium and we observed no increase in hnRNPA1 expression after FGF blockade (data not shown). Our data suggest that homeostatic FGF stimulation is essential for continued *let-7* expression but the mechanism of this effect is uncertain. *let-7* family, in turn, has been indirectly linked to the regulation of several TGFβ family members including TGFβR1 (Tzur et al., 2009).

Our study provides strong evidence supporting the link between FGF signaling, *let-7* expression and TGFβ. In cell culture studies, suppression of FGF signaling using several different approaches uniformly resulted in a marked (up to 120 fold) decrease in *let-7* expression. In vivo, *let-7* levels were dramatically decreased in embryos with reduced FGF signaling (FRS2α-2F mutants) while systemic administration of a pan-FGF trap, sFGFR1-IIIc, reduced *let-7* levels in endothelial cells from different organs. In each case, loss of FGF signaling-dependent *let-7* expression was associated with increased TGFβ family member expression, activation of TGFβ signaling and the appearance of Endo-MT markers.

The fact that the change in *let-7* levels itself and not some other effect of blocking FGF signaling is responsible for the upregulation of TGFβ signaling and Endo-MT is supported by a number of observations. In vitro studies show that reduction in *let-7* expression in EC induced by antagomirs, a pan-*let-7* sponge or expression of the *let-7* suppressor Lin28A leads to increased expression of TGFβ, TGFβR1 and classic TGF target genes such as collagen or vimentin. Furthermore, EC demonstrated a dramatic morphological change consistent with Endo-MT and expression of a number of smooth muscle and other mesenchymal markers. Similarly, in vivo antagomir suppression of *let-7*b/c expression also led to increased TGFβR1 expression and appearance of Endo-MT markers. Most importantly, restoration of *let-7*b levels in the endothelium using modified *let-7*b mimics and a delivery system designed to facilitate miRNA delivery to the endothelium, reversed the effect of FGF blockade or *let-7* antagomir treatment on expression of Endo-MT markers and

its functional consequences. While all *let-7* family members are expressed in EC, we chose *let-7*b because it demonstrates, along with *let-7*c, the most dramatic reduction in expression upon FGF signaling withdrawal and because of all *let-7 let-7*b has the best complementarity with TGFβR1 (Tzur et al., 2009).

The existence of an Endo-MT phenomenon still remains a matter of intense debate as are its contributions to human pathology. In addition to TGFβ, two other signaling pathway, Notch (Chang et al., 2011) and Tie-1 (Garcia et al., 2012), have also been reported to induce it. The molecular details, however, remain sparse. While there is a significant body of evidence linking TGFβ signaling to EMT, its role in Endo-MT is much less established. Several studies have reported that a prolonged stimulation of EC in vitro with TGFβ can induce Endo-MT (Ishisaki et al., 2003; Zeisberg et al., 2007a) but there are no studies demonstrating the ability of TGFβ to induce Endo-MT in vivo. TGFβ is thought to induce Endo-MT via Smad-dependent activation of Snail (Kitao et al., 2009). Endo-MT has been reported to occur in the setting of cardiac, renal, pulmonary, cancer and age-related fibrosis (Ghosh et al., 2010; Zeisberg et al., 2007a; Zeisberg et al., 2007b). The current study strongly supports the reality of an Endo-MT phenomenon and expands its biological role.

In particular, we have demonstrated that Endo-MT plays an important role in neointima formation, a process underlying a number of important cardiovascular disease states. In the transplant model, Endo-MT accounted for ~10% of SMC in the neointima while ~80% of luminal EC demonstrated mesenchymal transition. This is highly significant as, so transformed, these cells can be expected to secrete large amounts of collagen and other ECM proteins thus contributing to vessel fibrosis. Indeed, extensive fibrosis was evident in endothelial-specific FRS2α deletion or *let-7* antagomir administration. Furthermore, the acquisition of a mesenchymal phenotype by luminal EC is likely to lead to endothelial dysfunction, such as an increase vascular permeability or potentiate leukocyte transmigration (Murakami et al., 2008).

The trigger for the occurrence of Endo-MT is the loss of FGF signaling. While many factors can and do affect this process, the occurrence of FGF resistance is clearly associated with inflammation. We traced this link to the ability of key inflammatory mediators, including IFN-γ and TNF-α, to reduce FGFR1 expression and markedly decrease FGF-dependent ERK activation. Thus, conditions associated with intense vascular inflammation such as allogeneic artery transplantion, induce an extensive Endo-MT response. In other models of vascular injury where the loss of FGF signaling is less profound, such as wire artery injury or vein-to-artery grafting, Endo-MT still occurs but to a more limited extent. Beyond vascular injury, Endo-MT has been reported in a number of pathological settings including acute myocardial infarctions (Zeisberg et al., 2007b) and acute kidney injury (Basile et al., 2011) that are also characterized by an intense inflammatory component.

Most importantly, Endo-MT clearly occurs in human disease. Indeed, eight out of eight human arteries from chronically rejecting cardiac allografts demonstrated clear evidence of Endo-MT and human arteries transplanted into immunodeficient mice reconstituted with allogeneic human PBMC underwent Endo-MT with the same frequency as allogeneic mouse artery grafts.

In summary, FGF regulates endothelial TGFβ signaling by controlling TGFβ, TGFβR1 and Smad2 expression via control of *let-7* levels. The emergence of an FGF resistance state and a reduction in FGF signaling input leads to a profound decrease in *let-7* levels and increased TGFβ signaling culminating in Endo-MT that in turns leads to neointima formation and fibrosis.

Materials and methods

Primary mouse endothelial cell isolation and culture

Primary mouse endothelial cells were isolated from the heart and liver as described (Murakami et al, 2011).

let-7 family microsponge construction

A *let-7* microsponge of 273 nts was constructed containing nine bulged binding sites (one for each of the *let-7* family members: *let-7a, let-7b, let-7c, let-7d, let-7e, let-7f, let-7g, let-7i* and mir-98). The *let-7* family microsponge was synthesized by the annealing and ligation of 6 single-strand chemically synthetized DNA fragments. The bulged binding sites were designed using the canonic rules for microRNA binding sites (Filipowicz et al., 2008). The 273 nt *let-7* family microsponge was subcloned in tandem to multiply the binding sites.

Western blot analysis

Cells were lysed with T-PER (Thermo Scientific) containing complete mini protease inhibitors (Roche) and phosphatase inhibitors (Roche). 20 μg of total protein from each sample was resolved on a 4%–12% Bis-Tris Gel (Bio-Rad) with MOPs Running Buffer (Bio-Rad), transferred to nitrocellulose membranes (Bio-Rad) and probed with antibodies. Chemiluminescence measurements were performed using SuperSignal West Femto Maximum Sensitivity Substrate (Thermo Fisher Scientific).

RNA isolation, qRT-PCR, and gene expression profiling

RNA was isolated using RNeasy plus Mini Kit (Qiagen) and converted to cDNA using iScript cDNA synthesis kit (Bio-Rad). Quantitative real-time PCR (qRT-PCR) was performed using Bio-Rad CFX94 (Bio-Rad) by mixing equal amount of cDNAs, iQ SYBR Green Supermix (Bio-Rad) and gene specific primers. All reactions were done in a 25 μl reaction volume in duplicate. Data were normalized to endogenous β-actin. Primers are listed in Suppl Table 1.

Quantitative PCR analysis of 84 TGFβ related-and EMT-related genes was performed using Human TGFβ BMP signaling pathway (PAHS-035D, QIAGEN) RT^2 Profiler PCR Arrays and run on a Bio-Rad CFX96 machine (Bio-Rad). Data analysis was done using manufacturer's integrated web-based software package with cycle threshold (Ct)-based fold-change calculations.

MicroRNA target prediction

To identify potential miRNA binding sites within the 3'UTR of TGFβR1, the following bioinformatic databases were used: TargetScan (http://www.targetscan.org), PitTar (http://pictar.mdc-berlin.de), and DIANA-microT v3.0 (http://diana.cslab.ece.ntua.gr/).

microRNA real-time PCR analysis

Quantitative PCR analysis of 88 miRNA was performed using Human Cell Differentiation & Development RT^2 Profiler PCR Arrays (MAH-103A, QIAGEN). Validation of microRNA array data was performed with the RT^2 miRNA qPCR Assays and RT-PCR Primer Sets (QIAGEN). Individual miRNA expression was normalized in relation to expression of small nuclear SNORD47 (for human) or Snord66 (for mouse). PCR amplification consisted of 10 min of an initial denaturation step at 95°C, followed by 45 cycles of PCR at 95°C for 30 s, 60°C for 30 s.

Generation of mice and embryos

FRS2$^{flox/flox}$ (Lin et al., 2007) and FRS2α-2F (Gotoh et al., 2004) mice were previously described. Cdh5-CreERT2 (gift from R. H. Adams, Max Planck Institute, Munster) transgenic mice were crossed with mT/mG [B6,129(Cg)-Gt(ROSA)26Sor$^{tm4(ACTB-tdTomato,-EGFP)Luo}$/J] (JAX SN:007676) mice to generate EC-specific reporter mice. For fate mapping of Cdh5-GFP expressing cells, Cdh5CreERT2;mT/mG pups were pipette-fed with 0.05 mg/g tamoxifen solution (20 mg/ml stock solution in corn oil) every other day for 10 times.

let-7 miRNA lipid formulation

Synthesis of let-7b antagomirs. Antagomirs to *let-7*b and *let-7*c were synthesized as described (Krutzfeldt et al., 2005): anti-*let-7*b, 5'-a-$_s$a$_s$ccacacaaccuacuacc$_s$u$_s$c$_s$a$_s$-Chol-3'; and anti-*let-7*c, 5' a$_s$a$_s$ccauacaaccuacuacc$_s$u$_s$c$_s$g$_s$-Chol-3'. The lower case letters represent 2'-*O*Me-modified nucleotides; subscript 's' represents a phosphorothioate linkage; and 'Chol' represents cholesterol linked through a hydroxyprolinol linkage. Anti-*let-7*b and anti-*let-7*c were encapsulated in lipid nanoparticles (LNPs) using the same method and composition as previously described for C12-200-siRNA formulations (Love et al., 2010). Particle size was determined by dynamic light scattering (Zetasizer Nano ZS; Malvern, UK). The mean diameter for anti-*let7*b-LNP was 145 nm and for anti-*let7*c-LNP was 160 nm.

Synthesis of let-7b mimics

Chemically-modified miRNA mimics were synthesized at Alnylam Pharmaceuticals (Cambridge, MA). The sequences for the mature strands of *let-7*b after processing by Dicer, mmu-*let-7*b-5p (mmu-*let-7*b, MIMAT0000522), and mmu-*let-7*b-3p (mmus-*let-7*b*, MIMAT0004621), were obtained from the miRbase (http://www.miRbase.org). 2-*O*-methyl-nucleotide modifications (indicated in lower case) were introduced to both strands to decrease the likelihood of triggering an innate immune response. Double stranded miRNA mimics were obtained after annealing equimolar amounts of the chemically-modified 5p and 3p strands: mi-*let-7*b$_L$, for lightly modified (5p 5'-UGAGGuAGuAGGUUGUGUGGUU-3', 3p 5'-CuAuAcAACCuACUGCCUUCCC-3'); and mi-*let-7*b$_H$, for heavily modified, (5p 5'-UGAGGuAGuAGGUUGUGUGGUU-3', 3p 5'-cuAuAcAAccuAcuGccuuccc-3'). LNPs formulated with siRNA targeting luciferase, siLuc, were used as control.

miRNA formulation in lipid nanoparticles (LNPs)

microRNA mimics and siLuc were encapsulated in LNPs formulated with the lipid C12-200, using the same protocol and composition as previously described. The mean diameter range for all LNPs was 54–59 nm.

In vivo sFGFR1-IIIc adenovirus administration and let-7 antagomir delivery

sFGFR1-IIIc adenovirus (Murakami et al., 2008) was administered at a dose of 5×10^{10} viral particles per mouse via lateral tail vein injection. Control mice were given equivalent volumes of sterile PBS. Serum level of sFGFR1-IIIc was measured by a Human IgG Subclass Profile kit (Invitrogen). For *let-7* antagomir delivery, mice were administered with either 1:1 mixture of anti-*let7*b-LNP and anti-*let7*c-LNP or PBS at 2 mg/kg body weight in 0.1 ml per injection via lateral tail vein. Measurements of miRNA or mRNA levels in EC were performed 6 days after the injection.

In vivo let-7 antagomir and let-7 mimics delivery in mouse arterial transplant model

For *let-7* experiment, seven days after arterial transplant, mice were injected with four doses of *let-7* antagomir (2 mg/kg), luciferase-control (0.5 mg/kg), and *let-7*b mimics (0.5 mg/kg) in 0.1 ml per injection via jugular vein every other day.

Human tissue

De-identified human coronary arteries were obtained from organ donors with normal cardiac function, from end-stage cardiomyopathy patients undergoing heart transplantation, or from cardiac allograft recipients with chronic rejection at autopsy or undergoing re-transplantation. Tissue collection and analysis was approved by the review boards of Yale University School of Medicine, the New England Organ Bank, and the University of British Columbia.

Endo-MT animal models

All experiments were performed under protocols approved by Yale University Institutional Animal Care and Use and Human Investigation Committees.

Arterial transplant models

For mouse to mouse major mismatch arterial transplant model, segments of thoracic aorta from male, 4–5 week old BALBc/J mice were interposed into the infrarenal aortae of male recipient, 10–12 week old Cdh5CreERT2;mT/mG mice using an end-to-end microsurgical anastomotic technique. For human to mouse arterial transplant model, adjacent segments of human coronary artery from surgical specimens or cadaveric organ donors were implanted into the infrarenal aortae of 8-to 12-week-old CB.17 severe combined immunodeficient (SCID)/beige mice. The animals received 1×10^8 human allogeneic (to the artery) peripheral blood mononuclear cells (PBMC) per mouse, injected intraperitoneally 1 week after transplantation. Animals were euthanized 4 weeks after coronary artery transplantation and transplanted arteries were removed and frozen in OCT for further analysis.

Femoral artery injury model

This was done as described previously (Acevedo et al., 2004).

Vein graft model

For mouse vein to artery grafting model, segments of intrathoracic inferior vena cava from male, 4–5 week old C57BL/6 mice were interposed into the infrarenal aortae of male recipient, 10–12 week old Cdh5CreERT2;mT/mG mice using an end-to-end microsurgical anastomotic technique.

Morphometric analysis

To harvest transplanted grafts, artery, or liver, animals were anesthetized and tissues were perfused with normal saline and 4% PFA. For cryosection preparation, grafts were isolated from anesthetized mice, fixed in 4% paraformaldehyde (PFA) overnight at 4°C, cryoprotec ted 6 hr in 15% sucrose at 4°C and embedded in OCT (Tissue-Tek).

Immunofluorescence staining

Frozen blocks were sectioned at 6 μm intervals. For frozen tissue sections, slides were fixed in acetone for 10 min at −20°C. For paraffin sections, slides were dewaxed in xylene, antigen retrieval was performed by boiling for 20 min in citrate buffer (10 mM, pH 6.0), rehydrated. After washing three times with PBS, tissue sections were incubated with the following primary antibodies diluted in blocking solution (10% BSA and horse serum in PBS) overnight at 4°C in a humidified chamber: anti-human SM α-actin-APC (1:10); rabbit anti-Notch3 (1:100); rabbit anti-collagen 1 (1:100); rabbit anti-SM22α (1:100). Sections were washed three times with TBS, incubated with appropriate Alexa fluoro 488, 594, or 633 conjugated secondary antibodies diluted 1:1000 in blocking solution for 2 hr at room temperature, washed again three times, and mounted on slides with Prolong Gold mounting

reagent with DAPI (Invitrogen). Images were captured using Velocity software and quantifications performed using ImageJ (NIH).

Computer Assisted Image Analysis (Quantitative IF)

Pro-collagen and collagen positive area were measured using NIH Image 1.60. Neointima thickness was measured from 4 regions of a section along a cross, calculated the average from 5 serial cross-sections, 150 μm apart for each graft, using computer-assisted image analysis and NIH Image 1.60. For evaluation of αSMA^+/Cdh5-GFP^+ or $Notch3^+$/Cdh5-GFP^+ cells, at least 10 sections 150 μm apart per graft were analyzed for colocation of endothelial and smooth muscle markers using immunofluorescent staining imaged under 10× magnification.

Statistical analysis

Analysis was performed using GraphPad Prism software v.5. All data are presented as mean ±SD, and two group comparisons were done with a two-tailed Student's t-test. A value of $P<0.05$ was taken as statistically significant.

Supplementary Material

Refer to Web version on PubMed Central for supplementary material.

Acknowledgments

We thank R. Friesel (Maine Medical Center Research Institute) for providing FGFR1 constructs and FGFR1 antibody, R. Adams (Max Planck Institute, Munster) for Cdh5-CreERT2 mouse, V. Eswarakumar (Yale University) for the gift of FRS2α-2F mice, N. Kirkiles-Smith (Yale University) for technical assistance with i.v. injections, B. McManus (University of British Columbia) for human coronary artery specimens, and S. Kuchimanchi (Alnylam) for miR mimics synthesis.

This work was supported by National Institutes of Health Grants R01-HL 053793 (to M.S.) and R01-CA 131301 (to F.S.).

References

Acevedo L, Yu J, Erdjument-Bromage H, Miao RQ, Kim JE, Fulton D, Tempst P, Strittmatter SM, Sessa WC. A new role for Nogo as a regulator of vascular remodeling. Nature Medicine. 2004; 10:382–388.

Basile DP, Friedrich JL, Spahic J, Knipe N, Mang H, Leonard EC, Changizi-Ashtiyani S, Bacallao RL, Molitoris BA, Sutton TA. Impaired endothelial proliferation and mesenchymal transition contribute to vascular rarefaction following acute kidney injury. American journal of physiology Renal physiology. 2011; 300:F721–F733. [PubMed: 21123492]

Chang AC, Fu Y, Garside VC, Niessen K, Chang L, Fuller M, Setiadi M, Smrz J, Kyle A, Minchinton A, Marra M, Hoodless PA, Karasan A. Notch initiates the endothelial-to-mesenchymal transition in the atrioventricular canal through autocrine activation of soluble guanylyl cyclase. Developmental cell. 2011; 21:288–300. [PubMed: 21839921]

Chen PY, Simons M, Friesel R. FRS2 via fibroblast growth factor receptor 1 is required for platelet-derived growth factor receptor beta-mediated regulation of vascular smooth muscle marker gene expression. J Biol Chem. 2009; 284:15980–15992. [PubMed: 19339244]

Costa MA, Simon DI. Molecular basis of restenosis and drug-eluting stents. Circulation. 2005; 111:2257–2273. [PubMed: 15867193]

Eswarakumar VP, Lax I, Schlessinger J. Cellular signaling by fibroblast growth factor receptors. Cytokine Growth Factor Rev. 2005; 16:139–149. [PubMed: 15863030]

Fafeur V, Terman BI, Blum J, Bohlen P. Basic FGF treatment of endothelial cells down-regulates the 85-KDa TGF beta receptor subtype and decreases the growth inhibitory response to TGF-beta 1. Growth Factors. 1990; 3:237–245. [PubMed: 2173937]

Filipowicz W, Bhattacharyya SN, Sonenberg N. Mechanisms of post-transcriptional regulation by microRNAs: are the answers in sight? Nat Rev Genet. 2008; 9:102–114. [PubMed: 18197166]

Friesel R, Komoriya A, Maciag T. Inhibition of endothelial cell proliferation by gamma-interferon. J Cell Biol. 1987; 104:689–696. [PubMed: 3102503]

Garcia J, Sandi MJ, Cordelier P, Binetruy B, Pouyssegur J, Iovanna JL, Tournaire R. Tie1 deficiency induces endothelial-mesenchymal transition. EMBO reports. 2012; 13:431–439. [PubMed: 22421998]

Ghosh AK, Bradham WS, Gleaves LA, De Taeye B, Murphy SB, Covington JW, Vaughan DE. Genetic deficiency of plasminogen activator inhibitor-1 promotes cardiac fibrosis in aged mice: involvement of constitutive transforming growth factor-beta signaling and endothelial-to-mesenchymal transition. Circulation. 2010; 122:1200–1209. [PubMed: 20823384]

Gotoh N, Ito M, Yamamoto S, Yoshino I, Song N, Wang Y, Lax I, Schlessinger J, Shibuya M, Lang RA. Tyrosine phosphorylation sites on FRS2alpha responsible for Shp2 recruitment are critical for induction of lens and retina. Proc Natl Acad Sci U S A. 2004; 101:17144–17149. [PubMed: 15569927]

Hagan JP, Piskounova E, Gregory RI. Lin28 recruits the TUTase Zcchc11 to inhibit let-7 maturation in mouse embryonic stem cells. Nature structural & molecular biology. 2009; 16:1021–1025.

Hatanaka K, Simons M, Murakami M. Phosphorylation of VE-cadherin controls endothelial phenotypes via p120-catenin coupling and Rac1 activation. Am J Physiol Heart Circ Physiol. 2010; 300:H162–H172. [PubMed: 21037229]

Johnson CD, Esquela-Kerscher A, Stefani G, Byrom M, Kelnar K, Ovcharenko D, Wilson M, Wang X, Shelton J, Shingara J, et al. The let-7 microRNA represses cell proliferation pathways in human cells. Cancer Res. 2007; 67:7713–7722. [PubMed: 17699775]

Khurana R, Zhuang Z, Bhardwaj S, Murakami M, De Muinck E, Yla-Herttuala S, Ferrara N, Martin JF, Zachary I, Simons M. Angiogenesis-dependent and independent phases of intimal hyperplasia. Circulation. 2004; 110:2436–2443. [PubMed: 15477408]

Kitao A, Sato Y, Sawada-Kitamura S, Harada K, Sasaki M, Morikawa H, Shiomi S, Honda M, Matsui O, Nakanuma Y. Endothelial to mesenchymal transition via transforming growth factor-beta1/Smad activation is associated with portal venous stenosis in idiopathic portal hypertension. Am J Pathol. 2009; 175:616–626. [PubMed: 19608867]

Krutzfeldt J, Rajewsky N, Braich R, Rajeev KG, Tuschl T, Manoharan M, Stoffel M. Silencing of microRNAs in vivo with 'antagomirs'. Nature. 2005; 438:685–689. [PubMed: 16258535]

Lehrbach NJ, Armisen J, Lightfoot HL, Murfitt KJ, Bugaut A, Balasubramanian S, Miska EA. LIN-28 and the poly(U) polymerase PUP-2 regulate let-7 microRNA processing in Caenorhabditis elegans. Nature structural & molecular biology. 2009; 16:1016–1020.

Li Y, VandenBoom TG 2nd, Kong D, Wang Z, Ali S, Philip PA, Sarkar FH. Up-regulation of miR-200 and let-7 by natural agents leads to the reversal of epithelial-to-mesenchymal transition in gemcitabine-resistant pancreatic cancer cells. Cancer Res. 2009; 69:6704–6712. [PubMed: 19654291]

Lin Y, Zhang J, Zhang Y, Wang F. Generation of an Frs2alpha conditional null allele. Genesis. 2007; 45:554–559. [PubMed: 17868091]

Love KT, Mahon KP, Levins CG, Whitehead KA, Querbes W, Dorkin JR, Qin J, Cantley W, Qin LL, Racie T, et al. Lipid-like materials for low-dose, in vivo gene silencing. Proc Natl Acad Sci U S A. 2010; 107:1864–1869. [PubMed: 20080679]

Maller Schulman BR, Liang X, Stahlhut C, DelConte C, Stefani G, Slack FJ. The let-7 microRNA target gene, Mlin41/Trim71 is required for mouse embryonic survival and neural tube closure. Cell Cycle. 2008; 7:3935–3942. [PubMed: 19098426]

Medici D, Potenta S, Kalluri R. Transforming Growth Factor-beta2 promotes Snail-mediated endothelial-mesenchymal transition through convergence of Smad-dependent and Smad-independent signaling. Biochem J. 2011; 437:515–520. [PubMed: 21585337]

Michlewski G, Caceres JF. Antagonistic role of hnRNP A1 and KSRP in the regulation of let-7a biogenesis. Nature structural & molecular biology. 2010; 17:1011–1018.

Murakami M, Nguyen LT, Hatanaka K, Schachterle W, Chen PY, Zhuang ZW, Black BL, Simons M. FGF-dependent regulation of VEGF receptor 2 expression in mice. J Clin Invest. 2011; 121:2668–2678. [PubMed: 21633168]

Murakami M, Nguyen LT, Zhuang ZW, Moodie KL, Carmeliet P, Stan RV, Simons M. The FGF system has a key role in regulating vascular integrity. J Clin Invest. 2008; 118:3355–3366. [PubMed: 18776942]

Ohtani K, Egashira K, Hiasa K, Zhao Q, Kitamoto S, Ishibashi M, Usui M, Inoue S, Yonemitsu Y, Sueishi K, et al. Blockade of vascular endothelial growth factor suppresses experimental restenosis after intraluminal injury by inhibiting recruitment of monocyte lineage cells. Circulation. 2004; 110:2444–2452. [PubMed: 15477409]

Papetti M, Shujath J, Riley KN, Herman IM. FGF-2 antagonizes the TGF-beta1-mediated induction of pericyte alpha-smooth muscle actin expression: a role for myf-5 and Smad-mediated signaling pathways. Invest Ophthalmol Vis Sci. 2003; 44:4994–5005. [PubMed: 14578427]

Ramos C, Becerril C, Montano M, Garcia-De-Alba C, Ramirez R, Checa M, Pardo A, Selman M. FGF-1 reverts epithelial-mesenchymal transition induced by TGF-{beta}1 through MAPK/ERK kinase pathway. Am J Physiol Lung Cell Mol Physiol. 2010; 299:L222–L231. [PubMed: 20495078]

Rao DA, Eid RE, Qin L, Yi T, Kirkiles-Smith NC, Tellides G, Pober JS. Interleukin (IL)-1 promotes allogeneic T cell intimal infiltration and IL-17 production in a model of human artery rejection. The Journal of experimental medicine. 2008; 205:3145–3158. [PubMed: 19075290]

Reinhart BJ, Slack FJ, Basson M, Pasquinelli AE, Bettinger JC, Rougvie AE, Horvitz HR, Ruvkun G. The 21-nucleotide let-7 RNA regulates developmental timing in Caenorhabditis elegans. Nature. 2000; 403:901–906. [PubMed: 10706289]

Roush S, Slack FJ. The let-7 family of microRNAs. Trends Cell Biol. 2008; 18:505–516. [PubMed: 18774294]

Tzur G, Israel A, Levy A, Benjamin H, Meiri E, Shufaro Y, Meir K, Khvalevsky E, Spector Y, Rojansky N, et al. Comprehensive gene and microRNA expression profiling reveals a role for microRNAs in human liver development. PLoS One. 2009; 4:e7511. [PubMed: 19841744]

Urbich C, Kuehbacher A, Dimmeler S. Role of microRNAs in vascular diseases, inflammation, and angiogenesis. Cardiovasc Res. 2008; 79:581–588. [PubMed: 18550634]

Viswanathan SR, Daley GQ. Lin28: A microRNA regulator with a macro role. Cell. 2010; 140:445–449. [PubMed: 20178735]

Zeisberg EM, Potenta S, Xie L, Zeisberg M, Kalluri R. Discovery of endothelial to mesenchymal transition as a source for carcinoma-associated fibroblasts. Cancer Res. 2007a; 67:10123–10128. [PubMed: 17974953]

Zeisberg EM, Tarnavski O, Zeisberg M, Dorfman AL, McMullen JR, Gustafsson E, Chandraker A, Yuan X, Pu WT, Roberts AB, et al. Endothelial-to-mesenchymal transition contributes to cardiac fibrosis. Nature medicine. 2007b; 13:952–961.

Zhang B, Pan X, Cobb GP, Anderson TA. microRNAs as oncogenes and tumor suppressors. Dev Biol. 2007; 302:1–12. [PubMed: 16989803]

Highlights

1. FGF controls let-7 miRNA expression in endothelial cells
2. A reduction in let-7 expression leads to endothelial-to-mesenchyma transition (Endo-MT)
3. Endo-MT is an important contributor to human disease pathology

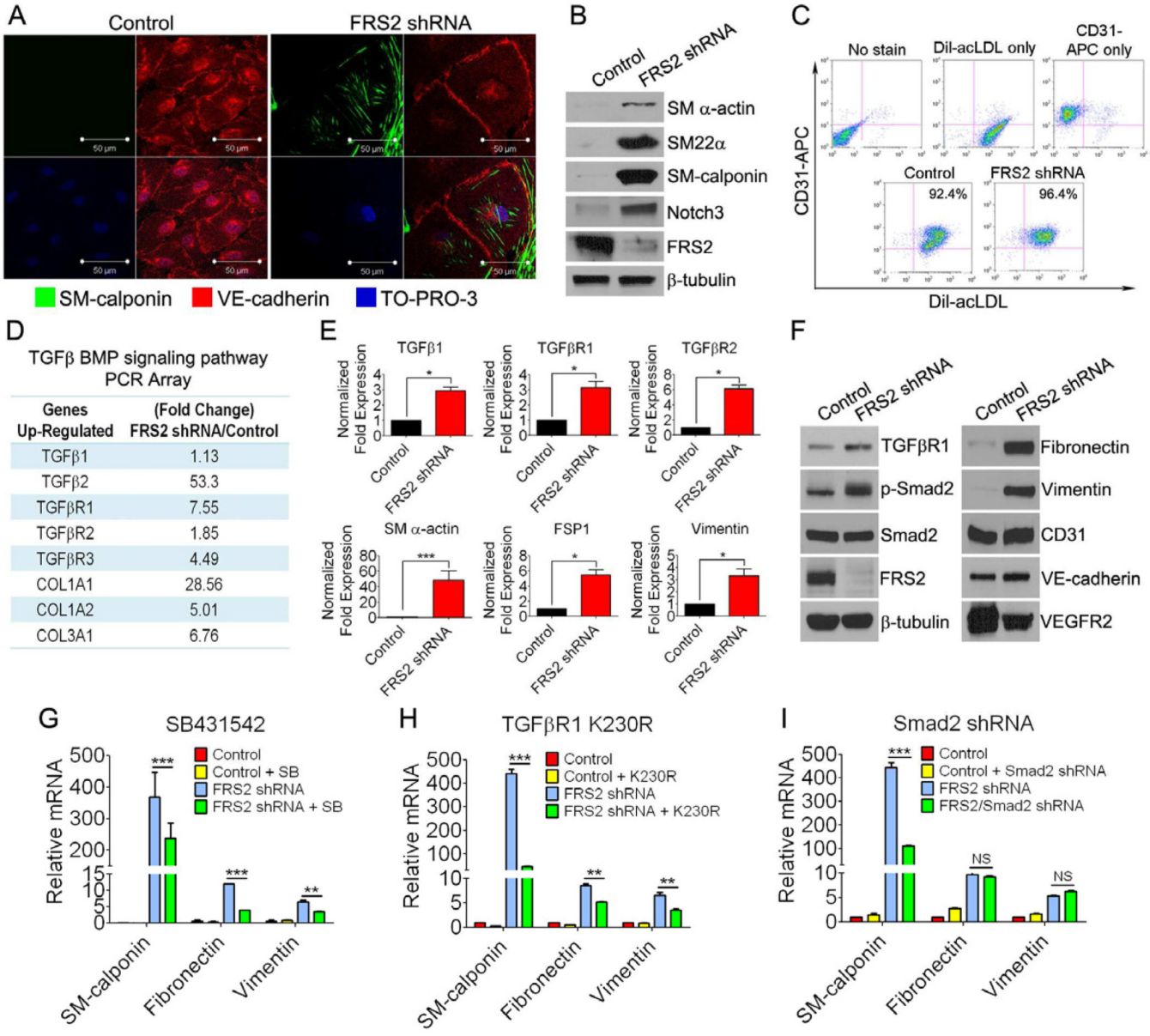

Figure 1. FRS2 regulates mesenchymal marker gene expression via the TGFβR1 pathway

(A) Immunofluorescence staining of VE-cadherin (red) and SM-calponin (green) in control and FRS2 knockdown HUAEC. Nuclei were counterstained with TO-PRO-3 (blue). Scale bar: 50 μm. (B) Immunoblots of SMC markers in control and FRS2 knockdown HUAEC. (C) Control or FRS2 knockdown HUAEC were analyzed by flow cytometry for CD31 and Dil-acLDL. (D) qPCR array mRNA expression profile of TGFβ family genes from control or FRS2 knockdown cells. (E) qRT-PCR analysis of TGFβRs and downstream target gene expression in control and FRS2 knockdown HUAEC. (*p<0.05; ***p<0.001 compared to control). β-actin was used to normalize the variability in template loading. (F) Immunoblots of TGFβR1, Smad2, mesenchymal, and endothelial cell markers in control and FRS2 knockdown HUAEC. (G–I) qRT-PCR analysis of SM-calponin and mesenchymal markers fibronectin and vimentin expression (**p<0.01; ***p<0.001; NS: not significant compared to control). β-actin was used to normalize the variability in template loading. Data shown are representative of four independent experiments (except (D)).

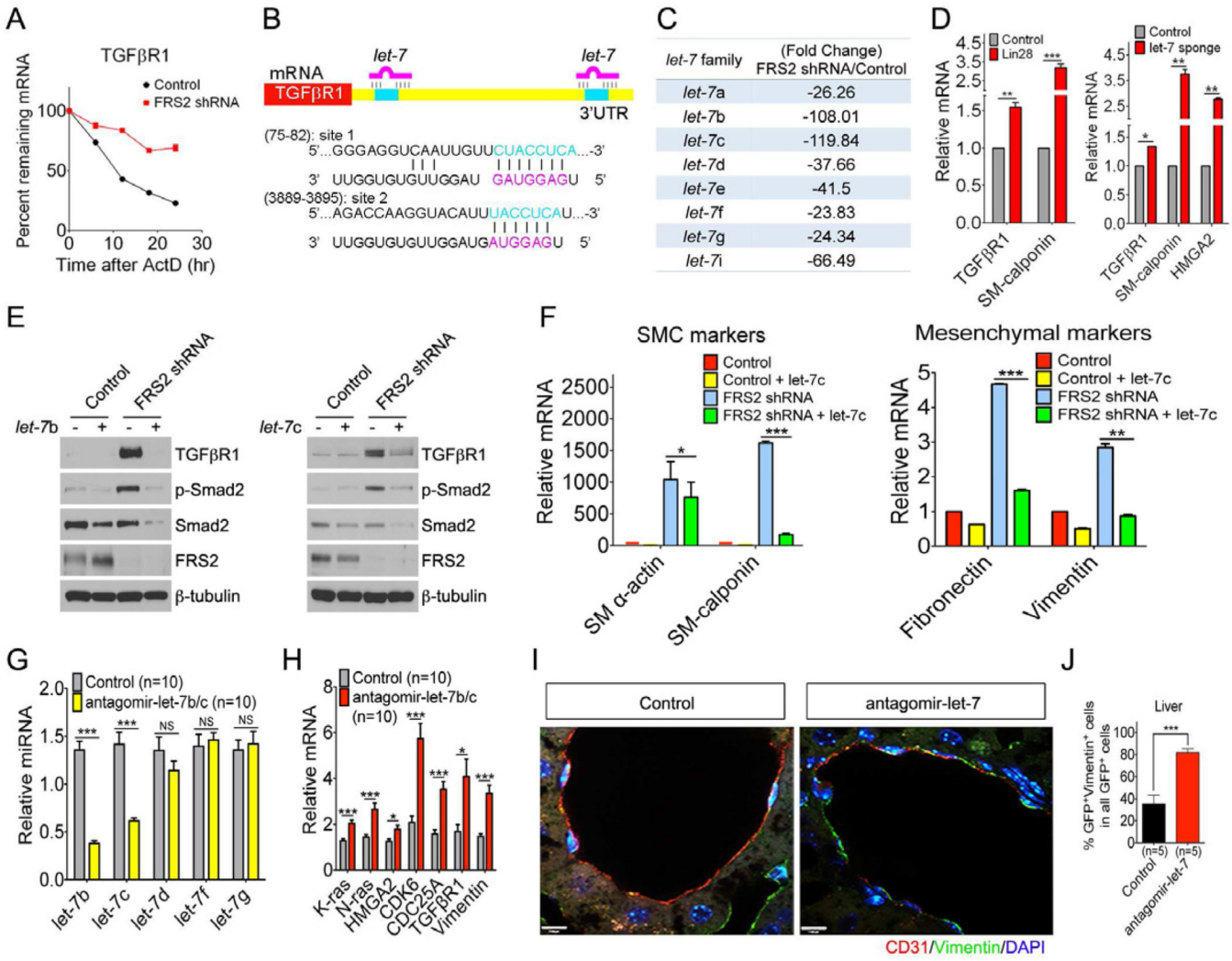

Figure 2. FRS2 knockdown downregulates let-7 family

(A) Control or FRS2 knockdown HUAEC were treated with DMSO or 10 μg/ml actinomycin D (ActD) for the indicated times. qRT-PCR was then used to determine TGFβR1 expression. 18S rRNA was used to normalize the variability in template loading. (B) Alignment of *let-7* sequences with the 3' UTRs of the human TGFβR1. (C) miRNA expression profiles assessed using real-time PCR miRNA arrays with cDNA from control or FRS2 knockdown cells. (D) qRT-PCR of TGFβR1 and SM-calponin in HUVEC transduced with Lin28, *let-7* sponge expressing-or empty vector. β-actin was used to normalize the variability in template loading. (E) Immunoblots of TGFβR1, p-Smad2, Smad2, and FRS2 in control and FRS2 knockdown HUAEC transduced with *let-7* lentiviruses. (F) qRT-PCR analysis of TGFβR1, TGFβ downstream target molecules, smooth muscle marker and mesenchymal marker gene expression in control and FRS2 knockdown HUAEC transduced with *let-7* lentiviruses (*p<0.05; **p<0.01; ***p<0.001 compared to control). β-actin was used to normalize the variability in template loading. Data shown (A and D–F) are representative of three independent experiments. (G) Mice were injected intravenously with control or cholesterol formulated antagomir-*let-7*b/c (single injection of 2 mg/kg) and the liver endothelial cells were isolated at 6 days. Expression of *let-7* miRNAs were analyzed by qRT-PCR. SNORD66 was used to normalize the variability in template loading (***p<0.001; NS: not significant compared to control). (H) Gene expression levels of K-ras,

N-ras, HMGA2, CDK6, CDC25A, TGFβR1, and vimentin in liver endothelial cells of mice treated with control or formulated antagomir-*let-7* at 6 days. β-actin was used to normalize the variability in template loading (*p<0.05; ***p<0.001 compared to control). (I) Immunofluorescence staining of CD31/vimentin (Nuclei were counterstained with DAPI (blue, scale bar: 7 μm.) in liver sections of mice treated with control or formulated antagomir-*let-7* at 6 days. (J) Quantification of liver EC express vimentin in mice injected with control or formulated antagomir-*let-7* (***p<0.001 compared to control).

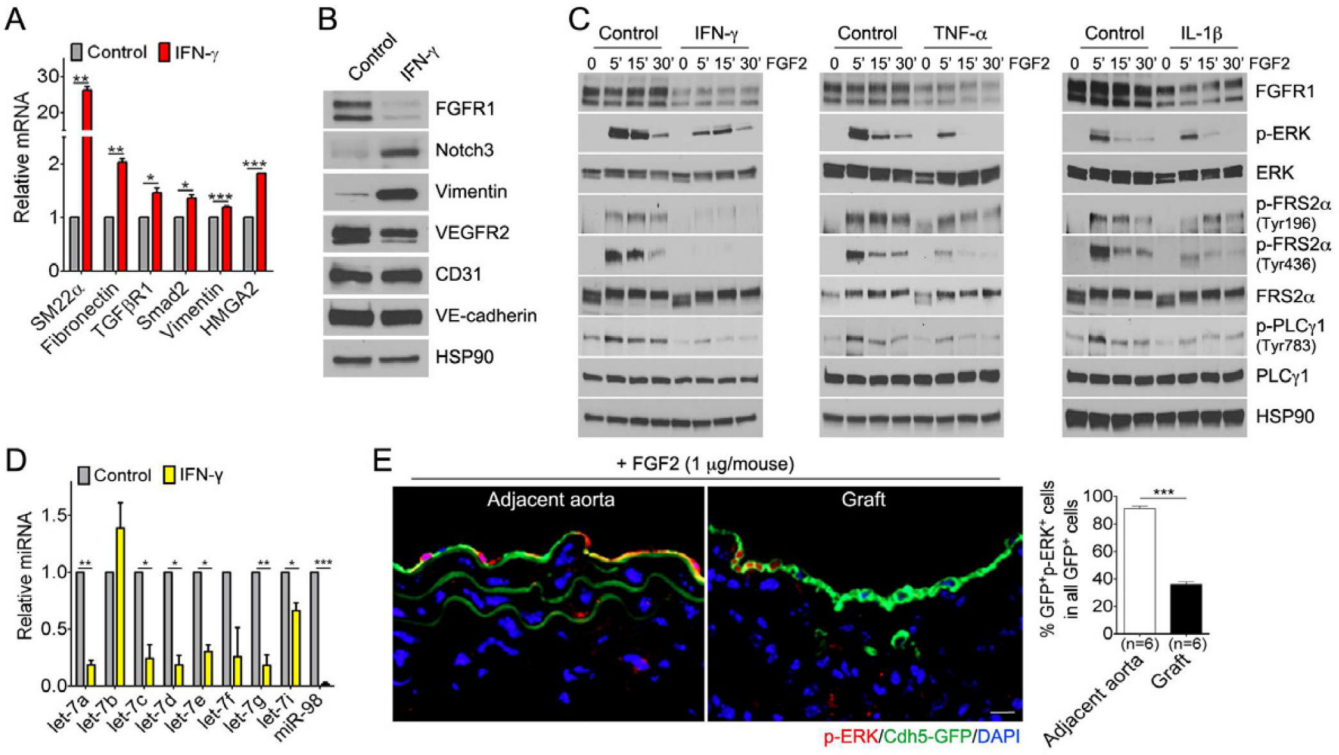

Figure 3. Inflammatory cytokines (IFN-γ, TNF-α, and IL-1β) downregulate FGF receptors, thereby rendering EC less responsive to FGF in vitro and in vivo

(A) qRT-PCR analysis of smooth muscle and mesenchymal marker gene expression in control and human IFN-γ treated HUVEC (*p<0.05; **p<0.01; ***p<0.001 compared to control). β-actin was used to normalize the variability in template loading. (B) Immunoblots of smooth muscle and mesenchymal markers in control and human IFN-γ treated HUVEC. (C) HUVEC were treated with human IFN-γ (10 ng/ml), human TNF-α (10 ng/ml), or human IL-1β (10 ng/ml) in complete growth medium for 6 days followed by incubation in 0.5% FBS starvation medium for 18 hr. Cells were treated with FGF2 (50 ng/ml) for indicated times. Immunoblots of FGF signaling downstream targets. (D) qRT-PCR analysis of mature *let-7* expression in control and human IFN-γ treated HUVEC. SNORD47 was used to normalize the variability in template loading. Data shown (A–D) are representative of four independent experiments. (E) Left: Immunofluorescence staining of p-ERK in adjacent aorta and graft sections in Cdh5-CreERT2;mT/mG mice. Scale bar: 10 μm. Right: Quantification of endothelial cell express p-ERK in mice injected with FGF2 (***p<0.001 compared to adjacent aorta).

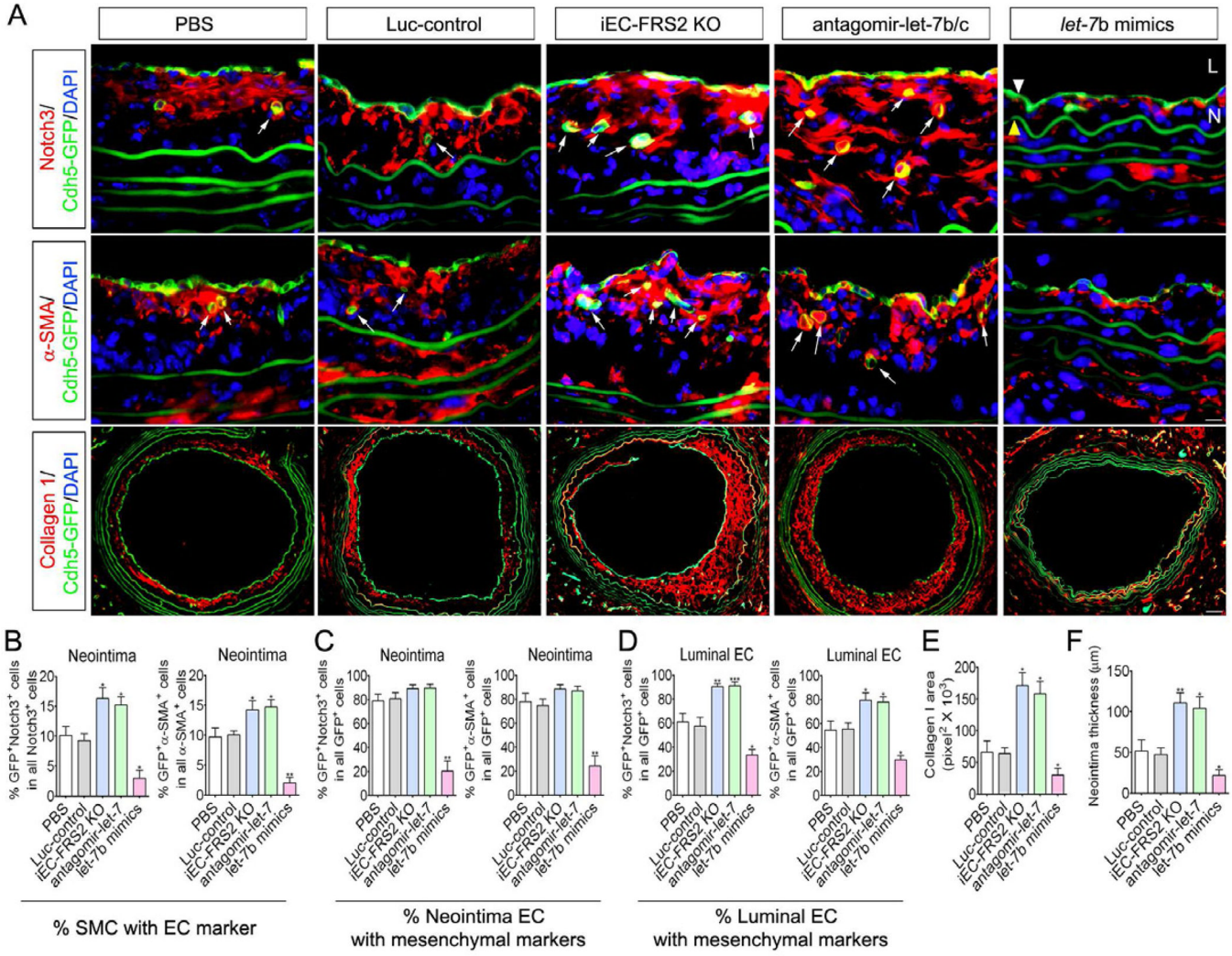

Figure 4. Endo-MT participates in mouse arteriosclerosis

(A) Histological analysis of artery grafts by immunostaining with anti-Notch3, anti-αSMA, and anti-collagen 1. Cdh5-GFP$^+$/Notch3$^+$ (red) and Cdh5-GFP$^+$/αSMA$^+$ (red) colocalization indicates Endo-MT and appears yellow. Nuclei were counterstained with DAPI (blue). Scale bar: 10 μm for Notch3 and αSMA and 63 μm for collagen 1. L, lumen; N, neointima; white triangle indicates endothelial cells; yellow triangle indicates IEL (internal elastic lamina); arrows indicate endothelial cells express SMC markers. (B) Percentage of Notch3$^+$ (left) or αSMA$^+$ (right) cells that were Cdh5-GFP$^+$ in neointima (*$p<0.05$; **$p<0.01$ compared to control). (C) Percentage of Cdh5-GFP$^+$ cells that were Notch3$^+$ (left) or αSMA$^+$ (right) in neointima (**$p<0.01$ compared to control). (D) Percentage of Cdh5-GFP$^+$ cells that were Notch3$^+$ (left) or αSMA$^+$ (right) in lumen (*$p<0.05$; **$p<0.01$; ***$p<0.001$ compared to control). (E–F) Morphometric assessment of collagen 1 area and artery graft neointima thickness was performed by computer-assisted microscopy (*$p<0.05$; **$p<0.01$ compared to control). PBS (N= 7 mice/group), Luc-control (N= 6 mice/group), iEC-FRS2KO (N= 4 mice/group), antagomir-*let-7* (N= 9 mice/group), and *let-7*b mimics (N= 6 mice/group).

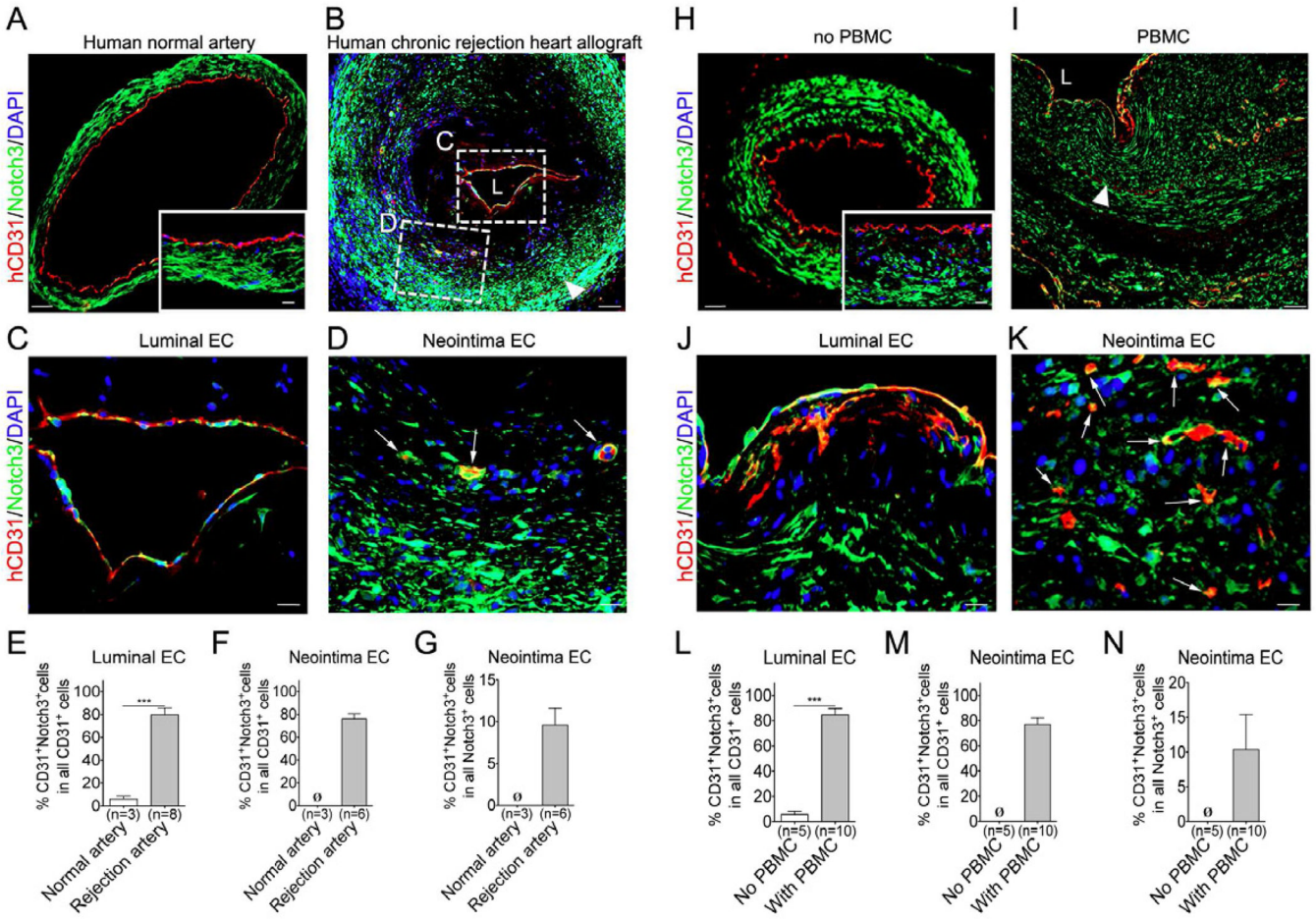

Figure 5. Endo-MT participates in human graft arteriosclerosis

(A–B) Representative images of human CD31 and Notch3 immunofluorescent staining of human normal and chronically rejecting human coronary arteries. Scale bar: 62 μm. L indicates lumen; white triangle indicates IEL (internal elastic lamina). (C–D) High-power images of human chronic rejection coronary artery lumen and neointima EC colocalized with Notch3 staining. Scale bar: 16 μm. Arrows indicate endothelial cells express SMC markers. (E) Percentage of $CD31^+$ cells that were $Notch3^+$ in lumen (***$p<0.001$ compared to normal artery). (F) Percentage of $CD31^+$ cells that were $Notch3^+$ in neointima (Ø, not detected). (G) Percentage of $Notch3^+$ cells that were $CD31^+$ in neointima (Ø, not detected). (H–I) Representative images of human CD31 and Notch3 immunofluorescent staining of human coronary artery transplants in SCID/beige mice reconstituted with or without human PBMCs. Scale bar: 62 μm. L indicates lumen; white triangle indicates IEL (internal elastic lamina). (J–K) High-power images of artery graft treated with human PBMC lumen and neointima EC colocalized with Notch3 staining. Scale bar: 16 μm. Arrows indicate endothelial cells express SMC markers. (L) Percentage of $CD31^+$ cells that were $Notch3^+$ in lumen (***$p<0.001$ compared to no PBMC). (M) Percentage of $CD31^+$ cells that were $Notch3^+$ in neointima (Ø, not detected). (N) Percentage of $Notch3^+$ cells that were $CD31^+$ in neointima (Ø, not detected).

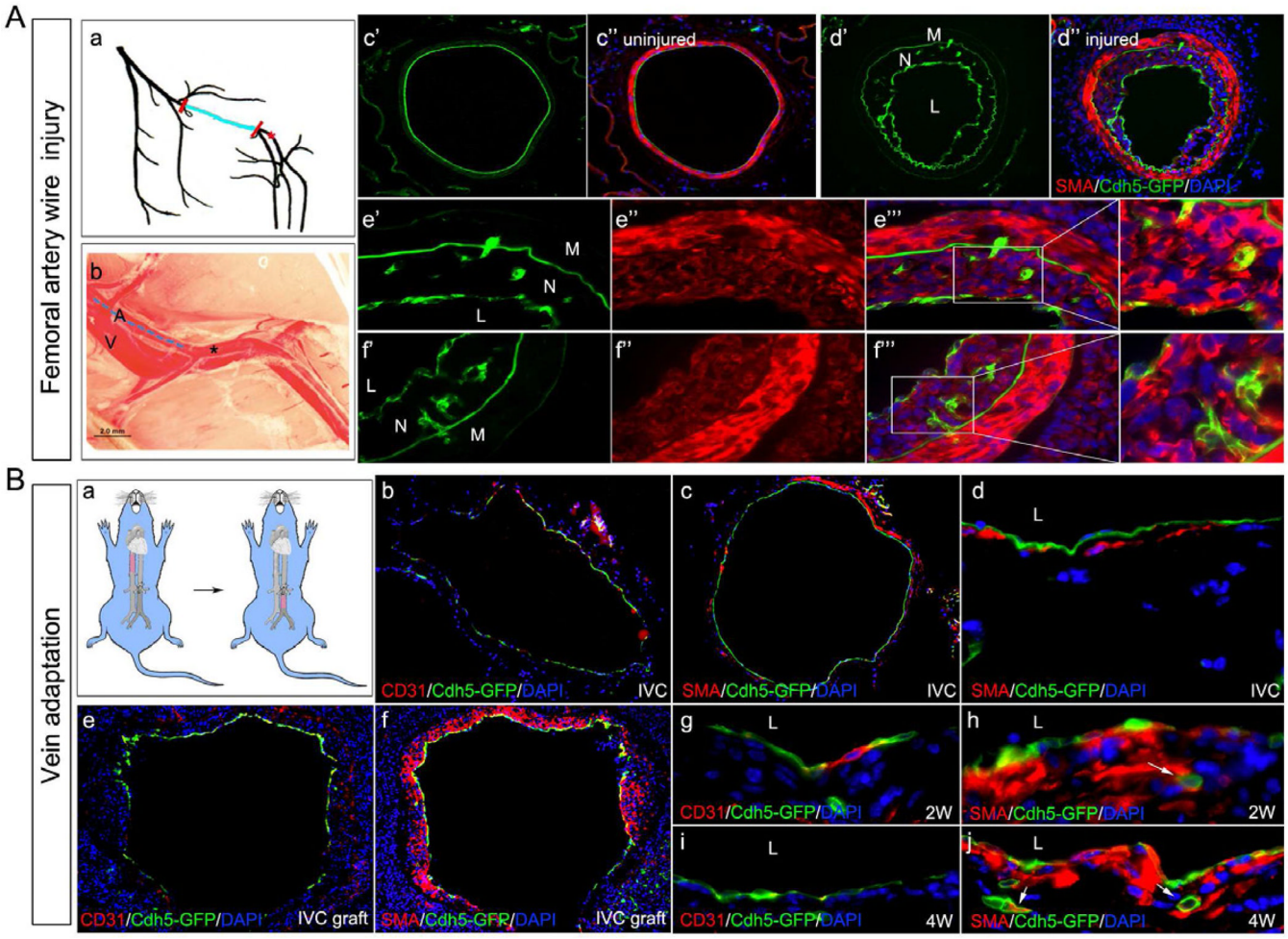

Figure 6. Endo-MT in femoral artery wire injury and vein adaptation models

(A) a–b: Anatomy of the hindlimb vasculature. Blue lines indicate denuded endothelium layer. A, artery; V, vein; asterisks indicate wire inserted site. c–d: Representative images of cross sections of the uninjured (left) and injured (right) femoral arteries. e–f: Immunofluorescence staining of αSMA (red) in injured femoral artery sections 3 weeks after injury. L, lumen; N, neointima; M, media. (B) a: Schematic of vein to artery grafting. b–c: Immunofluorescence staining of CD31 (red) and αSMA (red) in low power magnification of inferior vena cava (IVC). d: Immunofluorescence staining of αSMA (red) in high power magnification of IVC. e–f: Immunofluorescence staining of CD31 (red) and αSMA (red) in low power magnification of vein grafts. g&i: Immunofluorescence staining of CD31 (red) in high power magnification of vein grafts 2 and 4 weeks after transplantation. h&j: Immunofluorescence staining of αSMA (red) in high power magnification of vein grafts 2 or 4 weeks after transplantation.

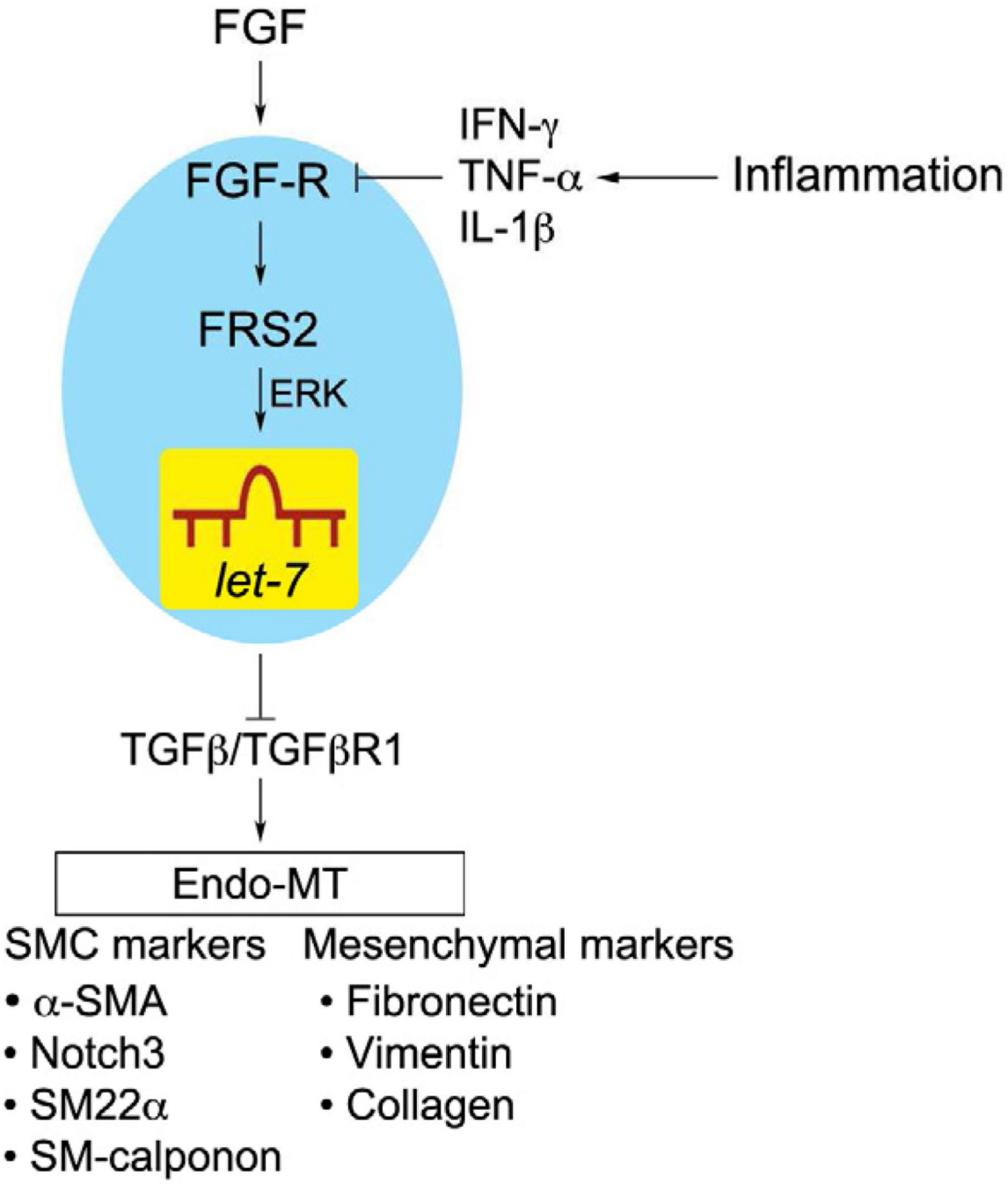

Figure 7. Schema of FGF-dependent regulation of TGFβ signaling and Endo-MT